Journal of
Materials Chemistry C

Accepted Manuscript

Single-source-precursor synthesis of high temperature stable SiC/C/Fe nanocomposites from a processible hyperbranched polyferrocenylcarbosilane with high ceramic yield

Zhaoju Yu,*[a] Le Yang, [a] Hao Min, [a] Pei Zhang, [a] Cong Zhou,[a] Ralf Riedel [b]

[a]College of Materials, Key Laboratory of High Performance Ceramic Fibers (Xiamen University), Ministry of Education, Xiamen 361005, China

[*] Corresponding author. E-mail: zhaojuyu@xmu.edu.cn

[b]Institut für Materialwissenschaft, Technische Universität Darmstadt, D-64287 Darmstadt, Germany

Abstract: Hydrosilylation of vinyl ferrocene with allylhydridopolycarbosilane was used to synthesize a processible hyperbranched polyferrocenylcarbosilane (HBPFCS), which was characterized by combination of gel permeation chromatography, Fourier transform infrared spectroscopy (FT-IR), and nuclear magnetic resonance (NMR). The polymer-to-ceramic transformation of the HBPFCSs was then investigated by FT-IR and ^{13}C MAS NMR spectroscopy as well as by thermal gravimetric analysis (TGA). A self-catalytic effect of ferrocenyl units in the HBPFCS skeleton on dehydrocoupling was found during a curing process at 170 °C resulting in a high ceramic yield of *ca.* 80% at 1200 °C in Ar. Finally, microstructures and magnetic properties of the final ceramics were studied by techniques such as X-ray diffraction, energy disperse spectroscopy, Raman spectroscopy, transmission electron microscopy and vibrating sample magnetometer. The final ceramic (pyrolysis temperature ≥ 900 °C) is characterized by a microstructure comprised of a SiC/C/Fe nanocomposite. Turbostratic carbon layers located at the segregated α-Fe crystal boundary avoids interdiffusion and explains the exclusive existence of α-Fe in a

SiC/C matrix even at 1300 °C. Variations of the iron content in the HBPFCSs and of the pyrolysis conditions facilitate control of the composition and ceramic micro/nanostructure influencing in particular magnetic properties of the final SiC/C/Fe nanocomposite ceramic.

1 Introduction

Incorporation of transition metals into Si-based polymer-derived ceramics (PDCs) may lead to the development of novel nanostructured materials with unique magnetic, electrical, and catalytic properties. [1-8] Among all transition metals, iron has the highest magnetic moment. Therefore, introduction of iron into Si-based PDCs is particularly preferred to include magnetic properties into the final ceramics. [9-13] Three different ways can be envisaged to introduce iron into Si-based ceramics derived from molecular routes: (i) blending of the precursor with iron or iron oxide powders,[14-16] (ii) synthesis from metallopolymers, [10-13, 17-24] and (iii) chemical modification of preceramic polymers using iron coordination compounds. [25-28] The first route is limited by the size of the used metal (oxide) powders, while in the case of (ii) and (iii) a bottom-up approach on the atomic scale, can be realized.[3]

Polyferrocenylsilane (PFS) is a relatively new class of metallopolymers, consisting of alternating ferrocene and organosilane units in their structural units. The PFS is a promising single-source-precursor (SSP) for SiFeC ceramics, which offers the possibility to tune the size of the in situ formed iron-based nanoparticles inside the derived PDCs by polymer tailoring. The first synthesis of high molecular weight PFS

via a ring-opening polymerization route was pioneered by Manners *et al.*, [29] then PFS with linear, [17, 18] hyperbranched [13, 19, 20] or cross-linked architecture [10, 21] and their block copolymers[22-24] have shown potential in the formation of shaped magnetic ceramics, the self-assembly into well-defined architecture such as micelle, sphere, cylinder, and one-dimensional nanostructure. Earlier work showed that upon pyrolysis of linear PFSs at 1000 °C gave low ceramic yields (17-56%), which were too low for shape retention.[18] As is well-known, an important consideration when choosing a ceramic precursor is the ceramic yield because this ultimately determines the utility, bulk properties, and shape retention in the resulting ceramics. To enhance ceramic yields, a cross-linked polyferrocenylsilanes (CPFS) network was explored in Manners' group. [20, 21] Because the ceramic yield of the CPFS network is higher than 90 wt% it provides a convenient route to process shaped and magnetically tunable ceramics. Cross-linked network polymers are, however, completely insoluble; as ceramic precursors, they suffer from the disadvantage of poor processibility while this feature is considered as one of the important advantages of the preceramic polymer processes. In this regard, Tang and co-workers [19, 20] synthesized a hyperbranched polyferrocenylsilane (HBPFS) precursor. Pyrolysis at high temperatures (1000-1200 °C) under nitrogen and argon generated ceramics in 48-62 wt% yields. More recently, Kong *et al.* [13] reported a novel strategy to synthesize nanostructured magnetoceramics *via* a direct bulk pyrolysis of hyperbranched polyferrocenyl(boro)carbosilanes with ceramic yield in the range of 25-40 wt%. With respective to the obtained ceramic microstructure by the SSP route, pyrolysis of this

kind of PFSs resulted in α-Fe or iron silicides (such as FeSi, Fe_3Si, or Fe_5Si_3) in a SiC-based matrix, [9-13, 19] which depended on the heating rate (slow heating of polymer resulted in α-Fe particles in a SiC/C while fast heating led to metastable ferromagnetic Fe_5Si_3) [11] or pyrolysis atmosphere (α-Fe particles on pyrolysis under nitrogen but crystalline Fe_3Si under argon).[10, 19] As mentioned above, it was inclined to form iron silicides in the resulting SiCFe ceramics, [9, 11-13, 19] which might be due to that SiC is chemically unstable at temperatures > 800 °C in the presence of iron to produce iron silicides and free carbon.[30]

Hyperbranched polymers are different from linear ones in terms of the dimensionality of molecular architecture, the former being three-dimensional spheres while the latter consists of one-dimensional chains. Hyperbranched preceramic polymers were found to be superior ceramic precursors in terms of the ceramic yield, if compared with those of the linear ones. [19] Recently, hyperbranched polycarbosilanes (HBPCSs) have drawn great attention as precursors to SiC. [31] In our previous work, we successfully synthesized a series of HBPCSs and studied their polymer-to-ceramic transformation systematically.[32-35] Interestingly, the HBPCSs are rich in reactive groups (*e.g.*, SiH, SiH_2, SiH_3, C=C, and/or C≡C groups). Therefore, we modified the HBPCS *via* reactions of the aforementioned reactive groups with borane, borazine, metal alkoxides, or metal complexes. [8, 36-40] The introduction of B and/or N, or metal significantly influences the microstructure and properties of the SiC-based ceramics.

Despite a few studies with respect to the HBPFS-based SSP, there is a lack of information concerning preparation of processibile hyperbranched

polyferrocenylcarbosilane (HBPFCS) *via* the third route, namely chemical modification of preceramic polymers using iron coordination compounds. With these considerations in mind, we tried to synthesize an HBPFCS by using $Fe(CO)_5$ to modify allylhydridopolycarbosilane (AHPCS). [40] Unfortunately, we failed to obtain the HBPFCS-based SSP since no direct evidence of Si-O-Fe or Si-Fe units in the resulting AHPCS-$Fe(CO)_5$ precursor was found by spectroscopic data. Instead, the reaction of Si-H bonds from the AHPCS with C=O groups evolved by $Fe(CO)_5$ decomposition occurred, which resulted in a cross-linked and insoluble polymer. In this work, we synthesized a novel HBPFCS *via* modification of allylhydridopolycarbosilane (AHPCS) by vinyl ferrocene (VF), and systematically investigated the polymer-to-ceramic transformation of the resultant HBPFCS as well as the relationship between nano/microstructure of the final ceramics and their properties. Interestingly, pyrolysis of our HBPFCS resulted in exclusive formation of α-Fe particles in SiC/C matrix even at a high temperature of 1300 °C, which was also clarified in detail.

2 Experimental methods

2.1 Materials

Allylhydridopolycarbosilane (AHPCS) with a formal composition $[SiH_{1.26}(CH_3)_{0.60}(CH_2CH{=}CH_2)_{0.14}CH_2]n$ was synthesized as previously reported by a one-pot synthesis with $Cl_2Si(CH_3)CH_2Cl$, Cl_3SiCH_2Cl, and $CH_2{=}CHCH_2Cl$ as the starting materials.[32] The AHPCS used in this work has a number average molecular

weight of ca. 600 and a polydispersity index of 1.8. Vinyl ferrocene [VF, 97%] was purchased from J & K and stored in fridge at 4 °C. Other commercially available reagents were used as received.

2.2 Polymer synthesis

All reactions were carried out in purified argon atmosphere using standard Schlenk techniques.[41] One typical synthesis of HBPFCS was described as the following procedure. 0.34 g VF was introduced into a 50 mL Schlenk flask in an argon atmosphere, and then 3.01 g AHPCS was introduced into the Schlenk flask with stirring at room temperature for 10 min, a pale red solution was obtained without any solvents. The hydrosilylation catalyst solution was prepared by mixing $H_2PtCl_6 \cdot 6H_2O$ and isopropyl alcohol at a weight ratio of 1/100. Subsequently, Pt catalyst solution was added into the AHPCS/VF solution with a weight ratio of 1/500 (H_2PtCl_6/AHPCS). Then, the reaction solution was heated up to 70 ℃ for 24 h under an argon flow. Finally, the unreacted VF was removed at 60 ℃ and under vacuum to give 3.20 g (a yield of about 95.8 %) of viscous dark red product. The weight ratios of Fe to AHPCS are 1%, 3%, and 5%, and the resultant polymers are abbreviated as HBPFCS-1, HBPFCS-3, HBPFCS-5, correspondingly. A control test was performed under the same conditions but no VF was added, and the resultant product is nominated as control AHPCS.

2.3 Polymer-to-ceramic transformation

In the present work, the resultant HBPFCS is a viscous polymer; therefore a curing of the sample at 170 °C for 6 h was used before pyrolysis. The curing process was carried out in an argon atmosphere, using 2 g samples in a Schlenk flask heated in a 170 °C oil bath. The control AHPCS transformed into a compact light yellow solid slowly, while the HBPFCS transformed into compact and stiff dark red solids immediately. The weight loss of polymers after 170 ^{o}C curing was slight (about 3 wt%). The Schlenk flask was then kept at 170 °C for 6 h. These cured polymers were used for both TGA and for macroscopic pyrolysis.

In order to understand the influence of temperature on the structural evolution during the polymer-to-ceramic transformation, the cured polymers were then pyrolyzed to various temperatures in a tube furnace. The cured sample was put in an alumina boat and heated in a glass silica tube under an argon flow. The samples were pyrolyzed as follows: heating up to the desired temperature (300, 600 or 900 °C) with a rate of 5 °C /min, hold for 2 h, followed by cooling down to room temperature.

According to TGA and FT-IR results the conversion of the precursors into the inorganic state is completed at a temperature close to 900 °C, so this temperature was selected for the synthesis of ceramics. After pyrolysis, the 900 °C ceramics were annealed at 1100 °C, 1200 °C, and 1300 °C, in argon atmosphere for 2 h in order to characterize the microstructure and properties. The 900 °C ceramic sample was put in a graphite crucible and heated in a tube furnace in argon, heated rapidly to the predetermined temperature at a rate of 5 °C/min and hold for 2 h, and finally cooled to room temperature.

Characterization

Gel permeation chromatography (GPC) (Agilent 1100 system, Agilent, Palo Alto, CA) measurements were performed at 35 °C with tetrahydrofuran as the eluant (1.0 mL/min). The spectrum was calibrated with narrow polystyrene standards. Fourier transform infrared spectroscopy (FT-IR) spectra were recorded on a Nicolet Avator 360 apparatus (Nicolet, Madison, WI) in the 4000-400 cm^{-1} frequently range, using KBr plates for liquid samples and KBr pellets for solid samples. In order to determine the reaction degree of the AHPCS/VF, the FT-IR spectra of the HBPFCSs were performed before the extraction of the unreacted VF from the reaction mixture. Nuclear Magnetic Resonance (NMR) experiments were carried out on a Bruker AV 300MHz spectrometer (Bruker, Germany) operating at 300.13 MHz for hydrogen-1, 75.46 MHz for carbon-13 (^{1}H-decoupling), and 59.63 MHz for silicon-29 (^{1}H decoupling), and the delay time is 30 s. The specimen used for NMR was dissolved in $CDCl_3$ solution. The ^{1}H, ^{13}C, and ^{29}Si chemical shifts were all referred to tetramethylsilane (TMS) (assigned to 0 ppm). The solid-state ^{13}C- magic angle spinning (MAS) NMR experiments were also performed on the Bruker AV 300 NMR spectrometer using a 4.0 mm Bruker double resonance MAS probe. The samples were spun at 5.0 kHz. The ^{13}C isotropic chemical shifts were referenced to the carbonyl carbon of glycine (assigned to 173.2 ppm). All the NMR spectra of the HBPFCSs were recorded after the extraction of the unreacted VF from the reaction mixture. Thermal behavior of the cured samples was performed on a thermal gravimetric

analysis (TGA) (Netzsch STA 409C, Netzsch, Germany) in argon gas with a heating rate of 10 °C/min ranging from room temperature to 1200 °C. X-ray diffraction (XRD) studies were executed on a PANalytical X'Pert PRO diffractometer (PANalytical, Netherlands), using graphite-monochromated Cu Kα radiation. The specimens were continuously scanned from 10° to 90° (2θ) at a speed of 0.0167° s^{-1}. Ceramic composition was determined by an energy disperse spectroscopy EDS (JAX-8100, Japan). Transmission electron microscopy (TEM) (JEM-2100, Japan) was used to observe the microstructure of the ceramics and was operated at 200 kV coupled with electron diffraction spectroscope (EDS, EDAX, USA). The TEM specimens were prepared by mechanical grinding. Raman spectra were recorded on a Horiba Jobin Yvon XploRa system. Magnetic properties of final ceramics were measured by using a vibrating sample magnetometer system (TOEIVSM-5-15, Japan) at room temperature (RT), and the standard sample is Ni. The Hk was determined by calculating the measured easy axis and hard axis loops of the reduced magnetization.

3 Results and discussion

3.1 Polymer characterization

In the present work, a series of HBPFCSs were synthesized by adjusting the weight ratio of Fe to the AHPCS in feed. The weight ratios of Fe to AHPCS are 1%, 3%, and 5%, and the resultant polymers are abbreviated as HBPFCS-1, HBPFCS-3, HBPFCS-5, correspondingly. In contrast, a control test was performed under the same conditions but no VF was added, and the resultant product is nominated as control

AHPCS. The synthesized polymers were subjected to GPC analysis to investigate the variation in their molecular weights. As shown in Fig. 1, there is no obvious change comparing the curve (a) with (b), indicating that no reaction occurred in case that parent AHPCS was treated at 70 °C without catalyst. Moreover, the number-average molecular weights (Mn) of the parent AHPCS, heat-treated AHPCS without catalyst, the control AHPCS and the HBPFCS-5 are 600, 630, 1000, and 870 g/mol, respectively. However, the molecular weight significantly increases in the presence of the H_2PtCl_6 / isopropyl alcohol mixture (a well-known hydrosilylation catalyst), suggesting that the Pt compound effectively catalyzes the self-hydrosilylation of the AHPCS bearing both C=C and SiHx (X= 1, 2, and 3) groups. For the HBPFCS-5, the molecular weight also increases compared with that of the parent AHPCS. Interestingly, the molecular weight of the HBPFCS-5 (curve (d)) is smaller than that of the control AHPCS (curve (c)) from the control test. The Pt-catalyzed self-hydrosilylation of the AHPCS leads to an increase in molecular weight, while the increase is significantly reduced with the introduction of VF into the AHPCS because the molecular weight of VF (212) is much smaller than that of the AHPCS (ca. 600). The GPC results indicate that a chemical reaction did occur between the AHPCS and the VF, and the reaction mechanism will be studied in more detail.

Fig.1.

The FT-IR spectra of the VF (a), parent AHPCS (b), unreacted AHPCS/VF mixtures (d, f, h), resultant HBPFCSs (e, g, i) and the AHPCS (c) from the control test are shown in Fig. 2. From a comparison of the FT-IR spectra of the HBPFCSs with

those of the parent AHPCS and VF, it is found that the HBPFCSs exhibit characteristic peaks of the parent AHPCS, while the characteristic peaks of ferrocenyl units are not obvious due to overlapping with the AHPCS vibration peaks. It is worth mentioning that the intensities of the C=C stretch (1630 cm^{-1}) absorption peak in the HBPFCSs decrease compared to those of the unreacted AHPCS/VF mixtures, indicating that the hydrosilylation did occur to consume the C=C groups. According to the previous work, [34, 35] there are three major reactions which can occur during the thermal cross-linking process of the AHPCS: (1) hydrosilylation (Si-H/C=C), (2) dehydrocoupling (Si-H/Si-H) and (3) vinyl polymerization (C=C/C=C). The hydrosilylation reaction is fast even at low temperatures (it starts at 100-120 °C), while dehydrocoupling and vinyl polymerizations start at higher temperatures (*ca.* 300 °C).[2] In the present work, it is presumed that only the hydrosilylation reaction occurred with a traditional Pt-catalyst, at such a low temperature of 70 °C. The consumption of the C=C bonds is due to the hydrosilylation reactions which occur between AHPCS/VF and/or AHPCS/AHPCS. In order to determine the reaction degree of the AHPCS/VF reaction mixture, FT-IR spectra of the HBPFCSs were performed before the extraction of the unreacted VF from the reaction mixture.

Fig.2.

According to the following equation, [33] we can determine the reaction degree of C=C ($P_{C=C}$) of the VF/AHPCS reaction mixture. Therefore, the $P_{C=C}$ includes both the reactions between AHPCS/VF and AHPCS/AHPCS, since the characteristic peaks of C=C groups of ferrocenyl units overlapps with the C=C groups of AHPCS vibration

peaks.

$$P_{C=C} = \frac{(A_{C=C}/A_{Si-CH_3})_{\text{unreacted}} - (A_{C=C}/A_{Si-CH_3})_{\text{reacted}}}{(A_{C=C}/A_{Si-CH_3})_{\text{unreacted}}}$$

Herein, the $(A_{C=C}/A_{Si-CH3})_{\text{unreacted}}$ indicates the intensity ratios of the peaks at 1630 cm^{-1} (C=C) to 1250 cm^{-1} (Si-CH_3) in the FT-IR spectra of the unreacted mixture. The $P_{C=C}$ of AHPCS is 11.21%, while those of HBPFCS-1, HBPFCS-3 and HBPFCS-5 are 15.51%, 20.03% and 31.31%, respectively. The $P_{C=C}$ values demonstrate that the reaction degrees of the AHPCS/VF mixtures increase with the increase in the iron proportions in the feed.

In order to further confirm the polymer architecture, NMR analysis was performed on the parent AHPCS, VF, unreacted AHPCS/VF mixtures and the resultant HBPFCSs. Taking HBPFCS-3 as an example, the ^{1}H NMR spectra are shown in Fig. 3. The ^{1}H NMR assignment of AHPCS has been described elsewhere.[32]

Fig.3.

As mentioned above, the self-hydrosilylation of the AHPCS did occur, which is responsible for the decrease in the intensities of the allyl-protons (g and h peaks) and SiH_3 peak (d peak) of the control AHPCS compared with that of the parent AHPCS. Technically, hydrosilylation involves addition of Si-H bonds to C=C bonds to generate β-addition and α-addition products, and the β-addition should be the dominant reaction. A new peak at 1.2 ppm is due to methylene protons related to $SiCH_2C\underline{\boldsymbol{H}}_2CH_2Si$ units derived from the β-addition product (eq 1), and peaks assigned to the methylene protons of $SiC\underline{\boldsymbol{H}}_2CH_2C\underline{\boldsymbol{H}}_2Si$ should be overlapped with proton peaks of the Si-$C\underline{\boldsymbol{H}}_3$/Si-$C\underline{\boldsymbol{H}}_2$ units (a+b peaks) of AHPCS.

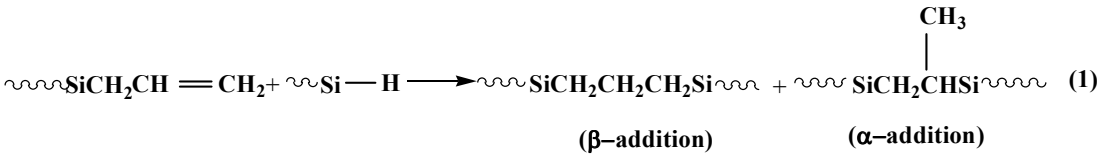

If compared with the unreacted AHPCS/VF mixture and the control AHPCS, the HBPFCS-3 shows a further decrease in the intensity of SiH_3 peak (d peak), indicating that the hydrosilylation between AHPCS and VF should occur besides the self-hydrosilylation of the AHPCS. In contrast to the control AHPCS, the intensity of the new peak at 1.2 ppm obviously increased due to the new-formed methylene protons of $SiCH_2C\boldsymbol{H}_2Cp$ (Cp: cyclopentadienyl) units in the presence of VF (eq 2).

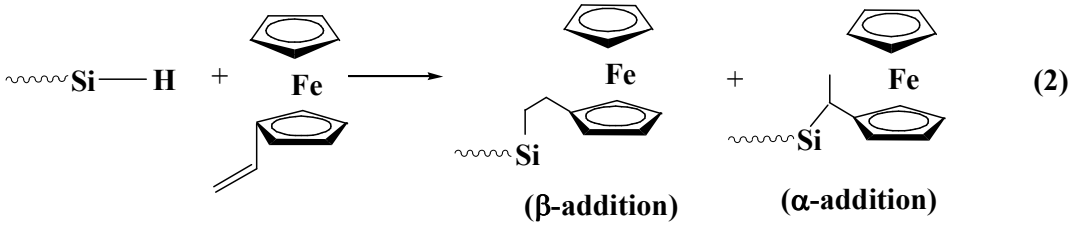

The $^{13}C\{^1H\}$ NMR spectra of the counterparts in Fig. 3 are shown in Fig. 4. The $^{13}C\{^1H\}$ NMR assignment of AHPCS has been described elsewhere, [32] and is depicted in Fig.4. Compared with the parent AHPCS, the intensities of the allyl-carbon signals (d and e) of the control AHPCS decrease due to the self-hydrosilylation. A new signal at 25 ppm appears due to the methylene carbon of $SiCH_2\underline{\boldsymbol{C}}H_2CH_2Si$ units from the β-addition product (eq 1), and signals assigned to the methylene carbon of $Si\underline{\boldsymbol{C}}H_2CH_2\underline{\boldsymbol{C}}H_2Si$ should be overlapped with those of the $Si\text{-}\underline{\boldsymbol{C}}H_3/Si\text{-}\underline{\boldsymbol{C}}H_2$ units (a+b signals) from the AHPCS. In contrast to the unreacted AHPCS/VF mixture and the control AHPCS, the HBPFCS-3 shows a significant increase in the intensity of the new signal at 25 ppm due to the methylene carbon of $SiCH_2\underline{\boldsymbol{C}}H_2Cp$ units formed in the presence of VF (eq 2). Moreover, the Cp signals of the HBPFCS-3 become

broader in comparison with those of the VF, which can be associated with a change in the Cp environment for carbon after hydrosilylation. The $^{13}C\{H\}$ NMR results are consistent with that of the ^{1}H NMR study, indicating that both the self-hydrosilylation of the AHPCS and the hydrosilylation between AHPCS and VF did occur in the AHPCS/VF reaction mixture to form the target compound HBPFCS.

Fig.4.

The $^{29}Si\{^{1}H\}$ NMR spectra of the AHPCS, control AHPCS and HBPFCS-3 are shown in Fig. 5. Complex multiplets centered at 5 ppm (tetraalkyl silicon, SiC_4), from -10 to -20 ppm (monohydridosilicon, C_3SiH), from -30 to -40 ppm (dihydridosilicon, C_2SiH_2) and from -55 to -60 ppm (trihydridosilicon, $CSiH_3$) evidence a branched structure,[32] indicating that iron modification did not change the hyperbranched structure. According to integration data, the relative values of $SiC_4/C_3SiH/C_2SiH_2/CSiH_3$ for the parent AHPCS, control AHPCS and HBPFCS-3 are about 1.31/0.69/0.74/1.00, 1.57/0.61/0.72/1.00, and 1.80/0.97/0.77/1.00, respectively. For the HBPCS-3, the content of $CSiH_3$ units decrease while that of SiC_4 units increase, due to the fact that the $CSiH_3$ unit is the most reactive species among the $C_{4-x}SiHx$ (x = 1, 2, or 3) units and took part in the hydrosilylation reaction to increase the number of SiC_4 units. The $^{29}Si\{H\}$ NMR results are in accordance with the ^{1}H NMR studies.

Fig.5.

According to the above-mentioned FT-IR and NMR results, the reaction between AHPCS and VF is given in Scheme 1. Both the self-hydrosilylation of AHPCS and

the hydrosilylation of AHPCS/VF occurred in the presence of the Pt catalyst at a low temperature of 70 ℃, leading to the successful synthesis of the HBPFCS polymers.

Scheme 1.

3.2 Polymer-to-ceramic transformation

Cross-linking preceramic polymers is a prevalent method for increasing the ceramic yield because it reduces the amount of volatile oligomers with low molecular weight. According to our previous work, [34, 35] the control AHPCS and the resulting HBPFCSs were cured at 170 ℃ for 6 h under an argon atmosphere before pyrolysis. The control AHPCS was slowly transformed into a yellow solid within 2 h, while the HBPFCSs were rapidly transformed into compact and stiff dark red solids within 10-20 min. This finding indicates that cross-linking of the HBPFCSs did occur and is improved by the introduction of VF, which is further confirmed by FT-IR (Fig. 6).

Fig.6.

It is found that the intensities of the Si-H peaks at 2100 cm^{-1} of the cured control AHPCS and HBPFCSs decrease in comparison with that of the control AHPCS. As discussed before, hydrosilylation reaction is fast even at low temperatures (it starts at 100-120 ℃), while dehydrocoupling and vinyl polymerization start at higher temperatures (*ca.* 300 ℃). During the curing process at a temperature of 170 ℃, hydrosilylation should be the dominative reaction. According to the semi-quantitative method,[33] the reaction degrees of Si-H (P_{Si-H}) of the preceramic polymers can be calculated according to the following equation:

$$P_{Si-H} = \frac{(A_{Si-H}/A_{Si-CH_3})_{\text{uncured}} - (A_{Si-H}/A_{Si-CH_3})_{\text{cured}}}{(A_{Si-H}/A_{Si-CH_3})_{\text{uncured}}}$$

Herein, the $(A_{Si\text{-}H}/A_{Si\text{-}CH3})_{\text{uncured}}$ indicates the intensity ratios of the peaks at 2100 cm^{-1} (Si-H) to 1250 cm^{-1} (Si-CH_3) in the FT-IR spectra of the control AHPCS and HBPFCSs, while the $(A_{Si\text{-}H}/A_{Si\text{-}CH3})_{\text{cured}}$ indicates those of the cured control AHPCS and cured HBPFCSs. Taking into account the formal composition $[SiH_{1.26}(CH_3)_{0.60}(CH_2CH{=}CH_2)_{0.14}CH_2]n$, a theoretical value for $P_{\text{Si-H}}$ of the parent AHPCS in the amount of *ca.* 11% is derived in case that hydrosilylation was involved during curing exclusively. However, the $P_{\text{Si-H}}$ of the cured control AHPCS, HBPFCS-1, HBPFCS-3 and HBPFCS-5 are 26.54%, 34.48%, 37.58%, and 44.52%**,** respectively. The results indicate that both hydrosilylation and dehydrocoupling reactions occured during the curing process, which is responsible for such a high value for $P_{\text{Si-H}}$. The number of $P_{\text{Si-H}}$ increases with the content of VF into the AHPCS skeleton. Therefore, the self-catalytic effect of the ferrocenyl units in AHPCS should not be ignored, which is supported by some reports that both dehydrocoupling and hydrosilylation could be effectively improved with bis(cyclopentadienyl)-metal complexes as catalysts.[42, 43]

As the preceramic polymer becomes insoluble upon cross-linking, solid-state NMR is an important method to investigate its molecular structure. The corresponding ^{13}C MAS NMR spectra of the VF, parent AHPCS and cured polymers are shown in Fig. 7. For the cured control AHPCS and HBPFCSs, the carbon signals from CH_2=CH- units of the parent AHPCS disappeared after curing, which is consistent

with the FT-IR results. In comparison with the ^{13}C MAS NMR spectrum of the cured control AHPCS, the HBPFCS spetra show one broad additional resonance around 68 ppm assigned to the Cp signals stemming from the ferrocenyl units of the HBPFCSs. The existence of Cp rings in the HBPFCSs further confirms that hydrosilylation between AHPCS and VF did occur. Moreover, the intensities of this resonance increase with the increase in VF content in the feed. Herein, ^{13}C MAS NMR spectra data has confirmed the presence of Cp and variation of the contents of Cp, which was not clearly resolved by FT-IR spectroscopy.

Fig.7.

The structural evolution during the polymer-to-ceramic conversion was studied exemplarily with the compound HBPFCS-3 by combination of FT-IR (Fig. 8) and ^{13}C MAS NMR (Fig. 9) studies. As discussed before, at 170 °C, the intensities of C=C overlapping peaks from AHPCS and VF reduce due to hydrosilylation, and that of Si-H peaks at 2100 cm^{-1} and 930 cm^{-1} decrease due to both hydrosilylation and dehydrocoupling. With the temperature increasing from 170 °C to 300 °C, the intensities of Si-H peaks significantly decreased, due to further cross-linking via dehydrocoupling (Si-H/Si-H). At 600 °C, the Si-H peaks almost vanish, indicating that the dehydrocoupling is almost completed. The intensities of the $Si-CH_3$ peaks at 2970 and 1250 cm^{-1} and $Si-CH_2-Si$ peaks at 2900 and 1350 cm^{-1} are reduced, which is attributed to the decomposition of the organic groups. At 900 °C, all the peaks related to organic groups including $Si-CH_2-Si$ and $Si-CH_3$ disappear. The broad peak at around 780 cm^{-1} and one weak peak at about 1100 cm^{-1} are retained and are attributed

to the amorphous SiC framework structure and Si-O-Si units, respectively. The latter is formed by the reactions of oxygen and moisture adsorbed on the surface of the polymers during the ceramization processes. Further heating from 1100 ℃ to 1300 ℃ leads to a sharpening of the Si-C band and a shift in its position from 780 cm^{-1} to 815 cm^{-1}, indicating the formation of crystalline SiC.[44]

Fig.8.

The ^{13}C MAS NMR spectra of HBPFCS-3 at different temperatures are shown in Fig. 9. After curing at 170 ℃, the broad resonance (68 ppm) assigned to the Cp signals from the polymer is retained. With the temperature increasing from 170 ℃ to 300 ℃, the intensity of the Cp broad resonance significantly decreases, suggesting that the decomposition of Cp occurred. At 600 ℃, the Cp signals are almost disappeared. In our case, the decomposition of Cp started from 170 ℃ and almost finished at 600 ℃. Interestingly, the Cp group confers sufficient stability to the metal complexes, and on the other hand, Cp can be eliminated at a relatively low temperature and provides a source of carbon when the temperature increases.

Fig.9.

In order to understand the thermal behavior during the polymer-to-ceramic transformation of the preceramic polymers, the TGA of the cured control AHPCS and HBPFCSs was measured and the result is shown in Fig. 10. Both, the control AHPCS curve and the HBPFCS-1 curve show the onset of thermal decomposition at ca. 300℃ while the HBPFCS-2 and HBPFCS-3 curves show the onset at ca. 200 ℃. At 300℃, weight losses of the control AHPCS and HBPFCS-1 amount 0.25 %, indicating that

the curing process is useful to reduce the evaporation of low molecular weight oligomers. The weight losses of the HBPFCS-2 and HBPFCS-3 are also low (1.5 %), due to the decomposition of the Cp rings in the polymers. For both control AHPCS and HBPFCS, it is shown that major weight loss takes place in the range of 300-900 °C, and no obvious weight loss occurs from 900 °C to 1200 °C. The results show that the polymer-to-ceramic transformation of our preceramic polymers is completed at ca. 900 °C, which is consistent with the FT-IR results. The ceramic yields of the HBPFCSs obtained at 900 °C are ca. 80 %, about 10 % higher than that of the control AHPCS (71.5 %). From 300 °C to 900 °C, the weight loss of the control AHPCS amounts 28.25 % while those of the HBPFCS-1, HBPFCS-3 and HBPFCS-5 are 21.55, 19.2 and 18.3 %, respectively. In the case of polycarbosilanes,[44] a quantitative GC analysis indicates that H_2 and CH_4 are the major volatile species evolved during pyrolysis, leading to the analyzed mass loss. It is well accepted that the dehydrocoupling (Si-H/Si-H) reactions lead to H_2 evolution. Therefore, compared with the cured control AHPCS, the Si-H contents of the cured HBPFCS are lower (Fig.6), resulting in less H_2 evolution and weight loss. It is worth mentioning that the ceramic yield increases with increasing VF concentration, due to the fact that lower Si-H contents were retained with more VF after curing at 170°C (Fig. 6).

Fig.10.

3.3 Ceramic microstructure

To investigate the crystallization behavior of the HBPFCS-derived ceramics, XRD

patterns of the samples were measured. Fig. 11 shows the variation of the crystallization behavior of the pyrolyzed products with increasing temperature. The sample annealed at 600 °C is amorphous and highly disordered, exhibiting no sharp reflection peaks. Further heating at 900 °C causes three broad peaks located at 2θ = 35.6°, 60.0° and 72.0°, corresponding to the (111), (220) and (311) lattice planes of β-SiC, respectively. In addition, the (002) reflection of graphite at 2θ = 26.0° appears. Progressive narrowing of the reflection of β-SiC was observed with further temperature increase. Heat treatment at 1100 °C causes a broad weak peak at 2θ = 45.2° in the XRD pattern of the pyrolyzed sample, corresponding to the (110) lattice plane of α-Fe.[14] The crystallization temperature of 1100 °C for α-Fe is significantly higher than that of the ceramics prepared from pyrolysis of cross-linked PFS (700 °C).[21] This finding may be caused by the difference in the iron content, which is supported by the fact that the α-Fe reflections appear at 1200 °C and 900 °C in the XRD patterns of the HBPFCS-1- and HBPFCS-5-derived ceramics, respectively (not shown). With increasing pyrolysis temperature, the reflection of α-Fe becomes sharper and more intense, which is attributed to the increased degree of crystallization and larger crystallite size. As shown in Fig. 8, the corresponding FT-IR spectra of the samples also show the dependence of the crystallization with temperature to be consistent with the XRD results. It is worth mentioning that crystallization of β-SiC is pronounced by the introduction of iron into the ceramic matrix, which may be due to the catalytic effect of iron on the decomposition of the SiCxOy phase. Phase decomposition will result in the evolution of gaseous CO and SiO, and the growth of

β-SiC crystals.[27]

Fig.11.

In addition, the effect of iron content on the crystallization behavior of the ceramics was also investigated. A series of samples containing different amounts of Fe synthesized at 1300 °C were prepared *via* the pyrolysis of our HBPFCSs with varying Fe content. The iron contents of the ceramics were calculated from their EDS spectra and the result is shown in Fig. 12. Accordingly, it is obvious that the iron content in the final ceramic increases linearly with the increase in the weight ratio of iron to AHPCS in the feed, indicating that the iron content in the ceramics can be readily controlled by varying the iron content in the precursor.

Fig.12.

Fig. 13 shows the XRD patterns of the respective samples given in Fig. 12. As the iron proportion increases in the polymer matrix, the intensities of the α-Fe peaks gradually increase, which reasonably well matches the increase of the iron content in the corresponding ceramics determined by EDS. Moreover, the peaks corresponding to that of the β-SiC phase become sharper as the iron content in the ceramics increases, because of the increased degree of crystallization. This finding clearly supports the catalytic effect of Fe on the decomposition of the Si-C-O phase.

Fig.13.

Raman spectroscopy is the key nondestructive tool for the examination of the structural evolution of the free carbon phase in polymer-derived ceramics. The representative features of free carbon in the Raman spectra of the resulting SiFeC

ceramics are the so-called disorder-induced D-band at *ca.* 1350 cm^{-1} and the G band at *ca.* 1582 cm^{-1} due to in-plane bond stretching of sp^2 carbon. [45] The appearance of the D and G bands confirms the existence of free carbon in the ceramic matrix, which is consistent with the XRD results shown in Fig. 11 and 13.

Fig. 14.

TEM is a powerful method in order to investigate the micro/nanostructure evolution of PDCs at different temperatures of annealing. Even if the PDCs are X-ray amorphous at low temperatures, they are typically heterogeneous as shown by TEM studies. [46] Therefore, the HBPFCS-3-derived SiFeC ceramics synthesized at different temperatures ranging from 600 to 1300 °C, were studied by means of TEM with respect to the evolution of its phase composition and microstructure upon ceramization (Fig. 15). The 600 °C sample shows no crystalline phases or segregated phase separation, which is also consistent with the XRD pattern. Electron diffraction shows a diffuse halo, indicative for an amorphous material. The sample annealed at 900 °C, however, reveals an obvious variation in contrast, as compared to the material pyrolyzed at 600 °C. Herein, the bright field lattice image shows, that dark and spherical iron nanoparticles are homogeneously dispersed in the ceramic matrix. As found by the selected area electron diffraction (SAED), the crystalline phases consist of SiC and α-Fe. High-resolution TEM (HRTEM) imaging exhibits the characteristic nanostructure of the ceramic where crystallites of β-SiC and α-Fe (*ca.* 5 nm), and poorly organized turbostratic carbon are dispersed in an amorphous SiC(O) matrix. With increasing annealing temperature, the SiFeC samples reveal an enhanced

crystallization as shown in the SAED inserts. In addition, the crystallites become bigger as can be taken from the bright field lattice images. According to the literature, SiC is chemically unstable at temperatures > 800 °C in the presence of iron due to reactions of iron with SiC to produce silicides and free carbon.[30] In our case, turbostratic carbon located at the α-Fe crystal boundary area hinders the interdiffusion and thus explains the existence of α-Fe in the SiC(O) matrix in the temperature range between 900 and 1300 °C. On the basis of the XRD studies, Raman spectroscopy and TEM results, the microstructure of our derived samples is characterized by a SiC/C/Fe nanocomposite.

Fig.15.

3.4 Magnetic properties

The formed α-Fe is the magnetic phase embedded in the amorphous SiC(O)/C matrix. The dependence of the magnetization behavior on the annealing temperature was studied representatively on the HBPFCS-3-derived ceramic by a vibration sample magnetometer system (VSMs). As shown in Fig. 16, the 600 °C sample (an organic/inorganic hybrid material) exhibits a weak magnetic behavior, since no iron crystallites are present in the matrix. The magnetization of the sample synthesized at 900 °C is more pronounced, which causes the ^{13}C MAS NMR experiment to give no signals (Fig. 9). The ceramic shows no hysteresis at RT, and the approach to magnetic saturation is slow, consistent with the behavior of superparamagnetic particles. According to the XRD and HRTEM results, the α-Fe particles become larger with

increasing annealing temperature from 900 to 1300 °C. Compared with the 900 °C ceramic, the ceramics annealed at higher temperatures rapidly reach saturation and display a hysteresis (with a small remanence of 0.07 emu g^{-1} for 1100 °C , 0.25 emu g^{-1} for 1200 °C and 0.36 emu g^{-1} for 1300°C) in their magnetization, which is consistent with a soft ferromagnet. This behavior is characteristic for a ceramic material in which the Fe nanoparticles have become large enough to display ferromagnetism. The VSM results thus demonstrate a transition from small superparamagnetic α-Fe particles to larger ferromagnetic α-Fe particles. Therefore, by varying the pyrolysis temperature, the α-Fe particle size and magnetic properties of the resultant ceramics can be tuned.

Fig.16.

In the case of the annealing temperature of 1300°C, the influence of the amount of iron of the ceramic on their magnetic properties was also investigated and the results are shown in Fig. 17. All the ceramics are magnetizable, while the pure AHPCS-derived ceramic is not (data not shown). The three Fe containing samples exhibit hysteresis loops with small remanent magnetization (0.07, 0.38 and 0.62 emu g^{-1} for HBPFCS-1, HBPFCS-3 and HBPFCS-5-derived ceramics, irrespectively), indicating soft ferromagnetism. It is analyzed that the saturation magnetization (Ms) amounts 0.48, 1.72, and 3.06 emu g^{-1} for the nanocomposite ceramics derived from HBPFCS-1, HBPFCS-3 and HBPFCS-5, respectively. Our results indicate that the saturation magnetization of the ceramics increases with increasing iron content in feed, which leads to higher iron contents in the final ceramics as shown in Fig.12. Thus, by

varying the iron contents in the feed, the iron contents and magnetic properties of the resulting nanocomposite ceramics can be adjusted.

Fig.17.

4 Conclusions

In this paper, a series of processible hyperbranched polyferrocenylcarbosilanes (HBPFCS) were synthesized by Pt-catalyzed hydrosilylation between AHPCS and VF under mild conditions. The polymer-to-ceramic transformation of the obtained HBPFCS and their relationship between the nano/microstructure of the final ceramics and their magnetic properties were investigated in detail. During a curing process at 170 °C, a self-catalytic effect of ferrocenyl units in the HBPFCS skeleton on dehydrocoupling has been found to be responsible for a high ceramic yield of *ca.* 80% at 1200 °C. The final ceramics (pyrolysis temperature ≥ 900 °C) consist of a microstructure of SiC/C/Fe nanocomposite in which α-Fe nanopaticles were homogeneously encapsulated in a SiC/C matrix. Turbostratic carbon layers located at the segregated α-Fe crystal boundary avoids interdiffusion and explains the existence of α-Fe in a SiC/C matrix at 900 to 1300 °C. By varying the iron content in the preceramic HBPFCS and pyrolysis temperature, the iron content, α-Fe particle size and magnetic properties of the formed ceramics could be tuned. This flexibility may be advantageous for particular materials application in many areas such as information storage and magnetic refrigeration.

Acknowledgements

This work was supported by the NSFC (Nos. 50802079 & 51072169) and Natural Science Foundation of Fujian Province of China (No. 2011J01330).

Notes and references

1. P. Colombo, G. Mera, R. Riedel and G. D. Soraru, *J. Am. Ceram. Soc.*, 2010，**93**, 1805.

2. E. Ionescu, H. J. Kleebe and R. Riedel, *Chem. Soc. Rev.*, 2012, **41**, 5032.

3. M. Zaheer, T. Schmalz, G. Motz and R. Kempe, *Chem. Soc. Rev.*, 2012, **41**, 5102.

4. I. Manners, *Science*, 2001, **294**, 1664.

5. E. Kockrick, R. Frind, M. Rose, U. Petasch, W. Boelhlmann, D. Gieger, M. Herrmann and S. Kaskel, *J. Mater. Chem.*, 2009, **19**,1543.

6. M. S. Bazarjani, H.-J. Kleebe, M. M. Müller, C. Fasel, M. B. Yazdi, A. Gurlo and R. Riedel, *Chem. Mater.,* 2011, **23**, 4112.

7. M. Zaheer, G. Motz and R. Kempe, *J. Mater. Chem.*, 2011, **21**,18825.

8. Z. J. Yu, H. Min, J. Y. Zhan and L. Yang, *Ceram. Int.*, 2013, **39**, 3999.

9. S. Bourg, B. Boury and R. J. P. Corriu, *J. Mater. Chem.,* 1998, **8**, 1001.

10. M. J. Maclachlan, M. Ginzburg, N. Coombs, T. W. Coyle, N. P. Raju, J. E. Greedan, G. A. Ozin and I. Manners, *Science*, 2000, **287**, 1460.

11. M. K. Kolel-Veetil, S. B. Qadri, M. Osofsky, R. Goswami and T. M. Keller, *J. Phys. Chem. C*, 2009, **113**, 14663.

12. V. A. Du, A. Sidorenko, O. Bethge, S. Paschen, E. Bertagnolli and U. Schubert, *J. Mater. Chem.*, 2011, **21**, 12232.

13. J. Kong, T. Schmalz, G. Motz and A. H. E. Müller, *J. Mater. Chem.*, 2013, **1**, 1507.

14. A. Francis, E. Ionescu, C. Fasel and R. Riedel, *Inorg. Chem.* 2009, **48**, 10078.

15. R. Hauser, A. Francis, R. Theismann and R. Riedel, *J. Mater. Sci.*, 2008, **43**, 4042.

16. A. Saha, S. R. Shah and R. Raj, *J. Mater. Res.*, 2003, **18**, 2549.

17. B. Z. Tang, R. Petersen, D. A. Foucher, A. Lough, N. Coombs, R. Sodhib and I. Manners, *J. Chem. Soc., Chem. Commun.,* 1993, 523.

18. R. Petersen, D. A. Foucher, B. Z. Tang, A. Laugh, N. P. Raju, J. E. Greedan and I. Manners, *Chem. Mater.*, 1995, **7**, 2045.

19. Q. Sun, J. W. Y. Lam, K. Xu, H. Xu, J. A. K. Cha, P. C. L. Wong, G. Wen, X. Zhang, X. Jing, F. Wang and B. Z. Tang, *Chem. Mater.*, 2000, **12**, 2617.

20. Q. H. Sun, K. T. Xu, H. Peng, R. H. Zheng, M. Haussler and B. Z. Tang, *Macromol.,* 2003, **36**, 2309.

21. M. Ginzburg, M. J. MacLachlan, S. M. Yang, N. Coombs, T. W. Coyle, N. P. Raju, J. E. Greedan, R. H. Herber,G. A. Ozin and I. Manners, *J. Am. Chem. Soc.*, 2002, **124**, 2625.

22. J. A. Massey, M. A. Winnik and I. Manners, *J. Am. Chem. Soc.*, 2001, **123**, 3147.

23. K. Kulbaba, A. Cheng, A. Bartole, S. Greenberg, R. Resendes, N. Coombs, A. Safa-Sefat, J. E. Greedan, H. D. H. St¨over, G. A. Ozin and I. Manners, *J. Am. Chem. Soc.*, 2002, **124**, 12522.

24. D. A. Rider, K. Liu, J.-C. Eloi, L. Vanderark, L. Yang, J.-Y. Wang, D. Grozea, Z.-H. Lu, T. P. Russell and I. Manners, *ACS Nano*, 2008, **2**, 263.

25. Y.M. Li, Z.M. Zheng, C.Y. Reng, Z.J. Zhang, W. Gao, S.Y. Yang and Z.M. Xie, *Appl. Organomet. Chem.*, 2003, **17**, 120.

26. Y.X. Yu, L.N. An, Y.H. Chen and D.X. Yang, *J. Am. Ceram. Soc.*, 2010, **93**, 3324.

27. X. J. Chen, Z. M. Su, L. Zhang, M. Tang, Y. Yu, L. T. Zhang, L. F. Chen, *J. Am. Ceram. Soc*., 2010, **93**, 89.

28. M. Hojamberdiev, R. M. Prasad, C. Fasel, R. Riedel, E. Ionescu, *J. Eur. Ceram. Soc.*, 2013, **33**, 2465.

29. D.A. Foucher, B.Z. Tang and I. Manners, *J. Am. Chem. Soc.*, 1992, **114**, 6246.

30. Y. Pan and J. L. Baptista, *J. Am. Ceram. Soc.* 1996, **79**, 2017.

31. L. V. Interrante, Q. H. Shen, In Silicon-Containing Dendritic Polymers, Dvornic P. R.; Owen M. J., Ed.; Springer Science + Business Media BV: Netherlands, 2009, 315-343.

32. T. H. Huang, Z. J. Yu, X. M. He, M. H. Huang, L. F. Chen, H. P. Xia and L. T. Zhang, *Chin. Chem. Lett.*, 2007, **18**, 754.

33. Y. H. Fang, M. H. Huang, Z. J. Yu, H. P. Xia, L. F. Chen, Y. Zhang and L. T. Zhang, *J. Am. Ceram. Soc.*, 2008, **91**, 3298.

34. H. B. Li, L. T. Zhang, L. F. Cheng, Y. G. Wang, Z. J. Yu, M. H. Huang, H. B. Tu and H. P. Xia, *J. Eur. Ceram. Soc.*, 2008, **28**, 887.

35. H. B. Li, L. T. Zhang, L. F. Cheng, Z. J. Yu, M. H. Huang, H. B. Tu and H. P. Xia, *J. Mater. Sci.*, 2009, **44**, 721.

36. Z. J. Yu, M. H. Huang, Y. H. Fang, R. Li, J. Y. Zhan, B. R. Zeng, G. M. He, H. P. Xia and L. T. Zhang, *React. Funct. Polym.* 2010, **70**, 334.

37. S. W. Li, L. T. Zhang, M. H. Huang, Z. J. Yu, H. P. Xia, Z. D. Feng and L. F. Cheng, *Mater. Chem. Phys.* 2012, **133**, 946.

38. Z. J. Yu, J. Y. Zhan, C. Zhou, L. Yang, R. Li and H. P. Xia, *J. Inorg. Organometallic Polym. Mater.* 2011, **24**, 412.

39. Z. J. Yu, L.Yang, J.Y. Zhan, C. Zhou, H. Min, Q. Zheng and H. P. Xia, *J. Eur. Ceram. Soc.* 2012, **32**, 1291.

40. Z.J. Yu, J.Y. Zhan, Z.H. Zhang, L.Yang, *Ceram. Int.*, 2013, **39**, 6945.

41. D. F. Shriver and M. A. Drezdzon, *The Manipulation of Air-Sensitive Compounds*, 2nd edition, Wiley, New York, 1986.

42. M. S. Cho, B. H. Kim, J. I. Kong, A. Y. Sung and H. G. Woo, *J. Organomet. Chem.*, 2003, **685**, 99.

43. M. Horacek, J. Pinkas, R. Gyepes, J. Kubista and K. Mach, *Organometallics*, 2008, **27**, 2635.

44. Q. Liu, H.J. Wu, R. Lewis, G.E. Maciel and L.V. Interrante, *Chem. Mater.,* 1999, **11**, 2038.

45. Y. Gao, G. Mera, H. N., K. Morita, H.-J. Kleebe and R. Riedel, *J. Europ. Ceram. Soc.*, 2012, **32**, 1857.

46. H. Bréquel, J. Parmentier, S. Walter, R. Badheka, G. Trimmel, S. Masse, J. Latournerie, P. Dempsey, C. Turquat, A. Desmartin-Chomel, L. Le Neindre-Prum, U.A. Jayasooriya, D. Hourlier, H.-J. Kleebe, G.D. Sorarù, S. Enzo and F. Babonneau, *Chem. Mater.* 2004, **16**, 2585.

Figure captions:

Scheme 1. Reaction of between AHPCS and VF to form hyperbranched polyferrocenylcarbosilane.

Fig.1. GPC traces of (a) parent AHPCS, (b) AHPCS (70°C, 24h) without catalyst, (c) control AHPCS (70°C, 24h) with catalyst, (d) HBPFCS-5.

Fig.2. FT-IR spectra of (a) VF, (b) parent AHPCS, (c) control AHPCS (70°C, 24h) with catalyst , (d) AHPCS/VF mixture with 1% Fe content, (e) HBPFCS-1, (f) AHPCS/VF mixture with 3% Fe content, (g) HBPFCS-3, (h) AHPCS/VF mixture with 5% Fe content, and (i) HBPFCS-5.

Fig.3. ^{1}H NMR spectra of VF, parent AHPCS, control AHPCS, unreacted AHPCS/VF mixture, and resultant HBPFCS-3.

Fig.4. $^{13}C\{^{1}H\}$ NMR spectra of VF, parent AHPCS, control AHPCS, unreacted AHPCS/VF mixture, and resultant HBPFCS-3.

Fig.5. $^{29}Si\{^{1}H\}$ NMR spectra of (a) parent AHPCS, (b) control AHPCS and (3) HBPFCS-3.

Fig.6. FT-IR spectra of (a) control AHPCS, (b) cured control AHPCS, (c) HBPFCS-1, (d) cured HBPFCS-1, (e) HBPFCS-3, (f) cured HBPFCS-3, (g) HBPFCS-5, and (h) cured HBPFCS-5 at 170 °C in Ar.

Fig.7. ^{13}C NMR spectra of (a) VF, (b) parent AHPCS, and solid-state ^{13}C MAS NMR spectra of cured (c) control AHPCS, (d) HBPFCS-1, (e) HBPFCS-3, (f) HBPFCS-5 at 170 °C in Ar.

Fig.8. FT-IR spectra of HBPFCS-3 heat treated at different temperatures in Ar.

Fig.9. ^{13}C NMR spectrum of (a) HBPFCS-3 and solid-state ^{13}C MAS NMR spectra of samples pyrolyzed at various temperatures in Ar: (b) 170 °C, (c) 300 °C, and (d) 600 °C.

Fig.10. TGA curves of cured (a) control AHPCS, (b) HBPFCS-1, (c) HBPFCS-3, and (d) HBPFCS-5.

Fig.11. XRD patterns of HBPFCS-3-derived samples pyrolyzed at different temperatures.

Fig.12. Dependence of the Fe content in the ceramics synthesized at 1300 °C on the iron content in feed.

Fig.13. XRD patterns of 1300 °C ceramics derived from (a) control AHPCS, (b) HBPFCS-1, (c) HBPFCS-3, and (d) HBPFCS-5.

Fig. 14. Raman spectra of HBPFCS-3-derived ceramics at different temperatures.

Fig.15. (a) Bright field lattice images (insets: selected area electron diffraction) and (b) HRTEM images of HBPFCS-3-derived ceramics annealed at different temperatures (insets: diffraction patterns obtained by Fourier filtered transformation).

Fig.16. Magnetization versus applied magnetic field for HBPFCS-3-derived ceramics at different temperatures (inset: enlarged portion of the plots at low H).

Fig.17. Magnetization versus applied magnetic field for 1300 °C ceramics derived from (a) HBPFCS-1, (b) HBPFCS-3, and (c) HBPFCS-5. (inset: enlarged portion of the plots at low H)

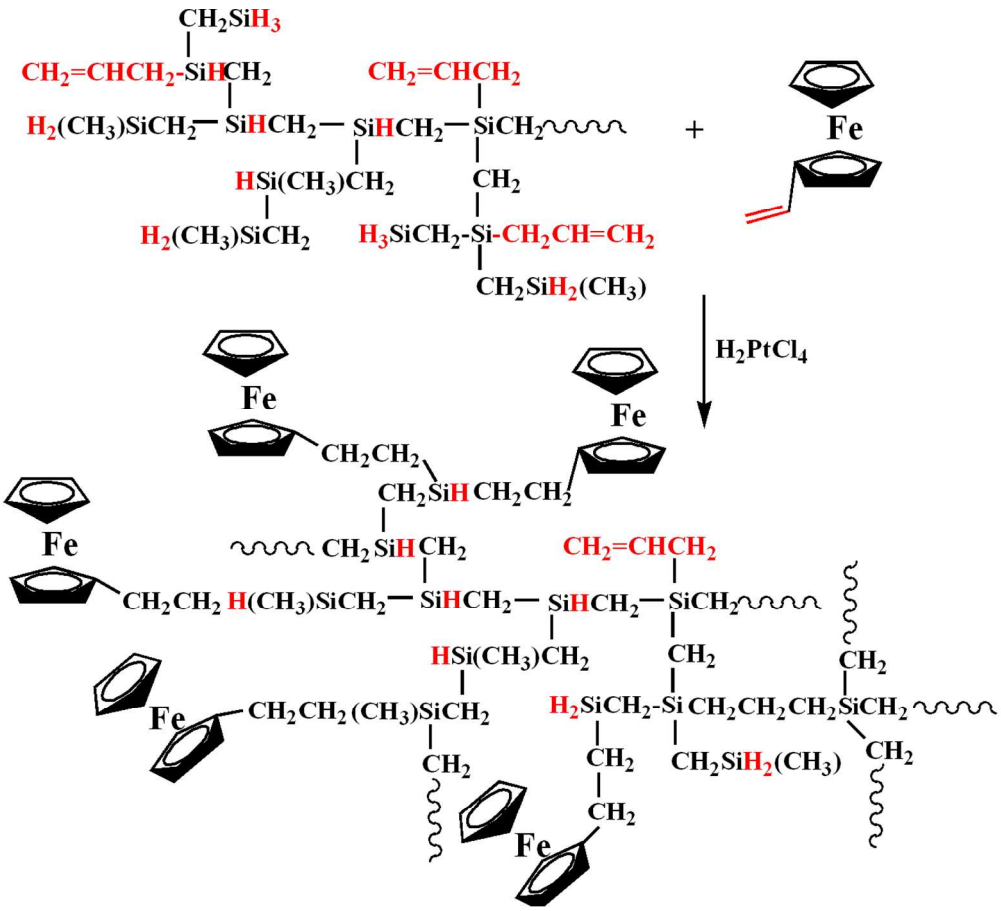

Scheme 1. Reaction of between AHPCS and VF to form hyperbranched polyferrocenylcarbosilane.
120x108mm (300 x 300 DPI)

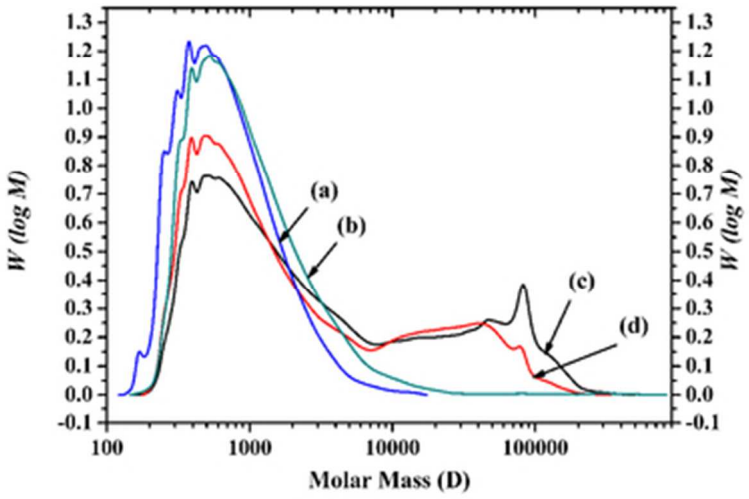

Fig.1. GPC traces of (a) parent AHPCS, (b) AHPCS (70°C, 24h) without catalyst, (c) control AHPCS (70°C, 24h) with catalyst, (d) HBPFCS-5.
34x24mm (300 x 300 DPI)

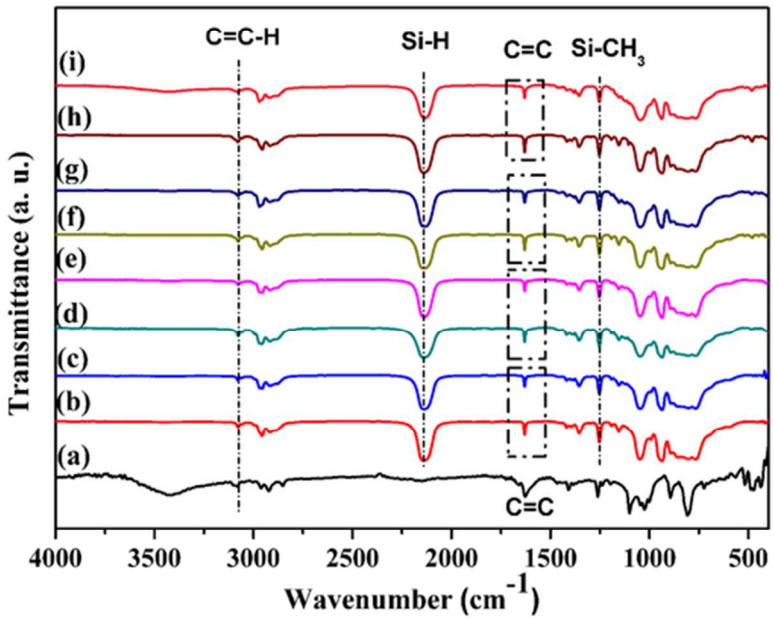

Fig.2. FT-IR spectra of (a) VF, (b) parent AHPCS, (c) control AHPCS (70°C, 24h) with catalyst , (d) AHPCS/VF mixture with 1% Fe content, (e) HBPFCS-1, (f) AHPCS/VF mixture with 3% Fe content, (g) HBPFCS-3, (h) AHPCS/VF mixture with 5% Fe content, and (i) HBPFCS-5.
55x39mm (300 x 300 DPI)

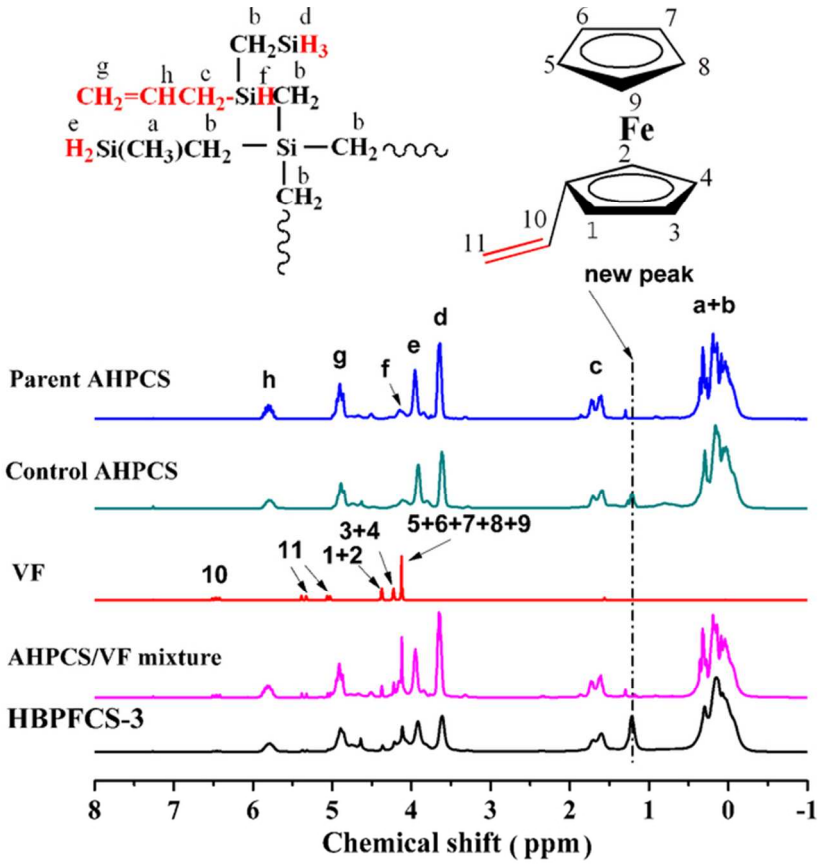

Fig.3. 1H NMR spectra of VF, parent AHPCS, control AHPCS, unreacted AHPCS/VF mixture, and resultant HBPFCS-3.
70x61mm (300 x 300 DPI)

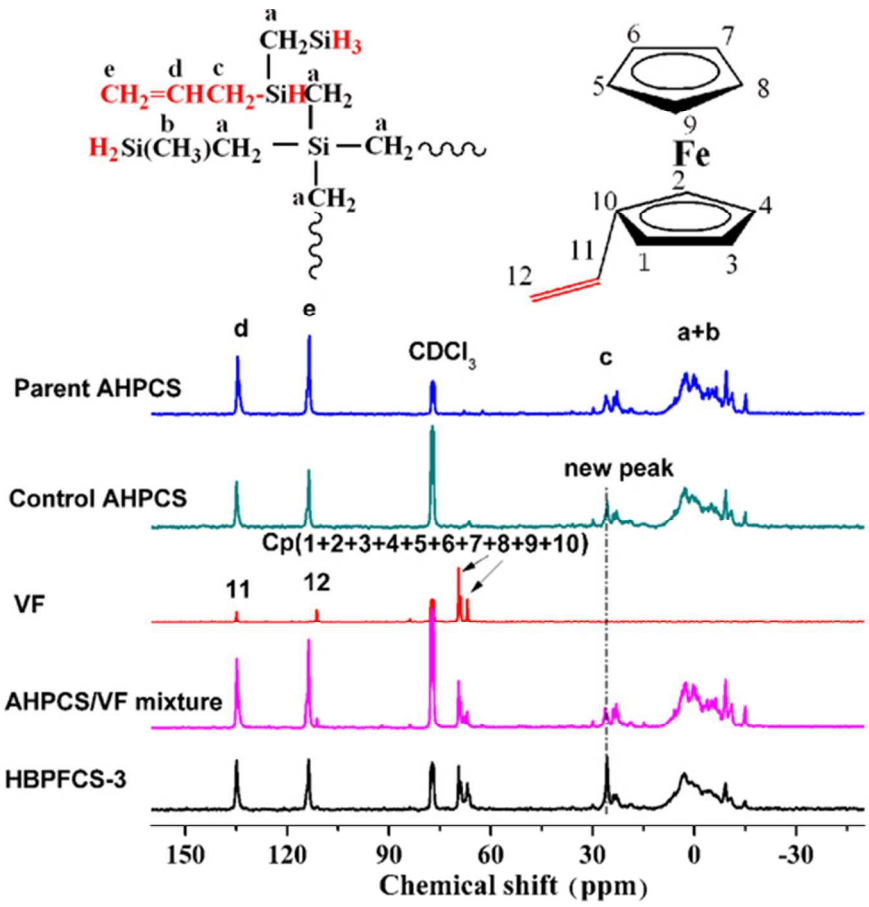

Fig.4. 13C{1H} NMR spectra of VF, parent AHPCS, control AHPCS, unreacted AHPCS/VF mixture, and resultant HBPFCS-3.
54x50mm (300 x 300 DPI)

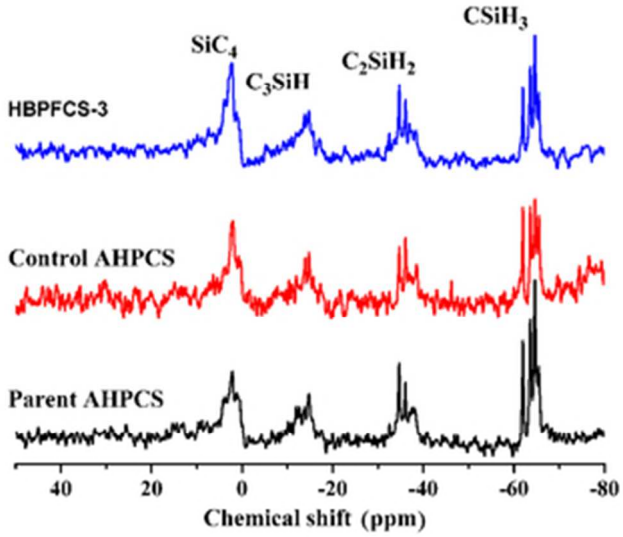

Fig.5. 29Si{1H} NMR spectra of (a) parent AHPCS, (b) control AHPCS and (3) HBPFCS-3.
34x24mm (300 x 300 DPI)

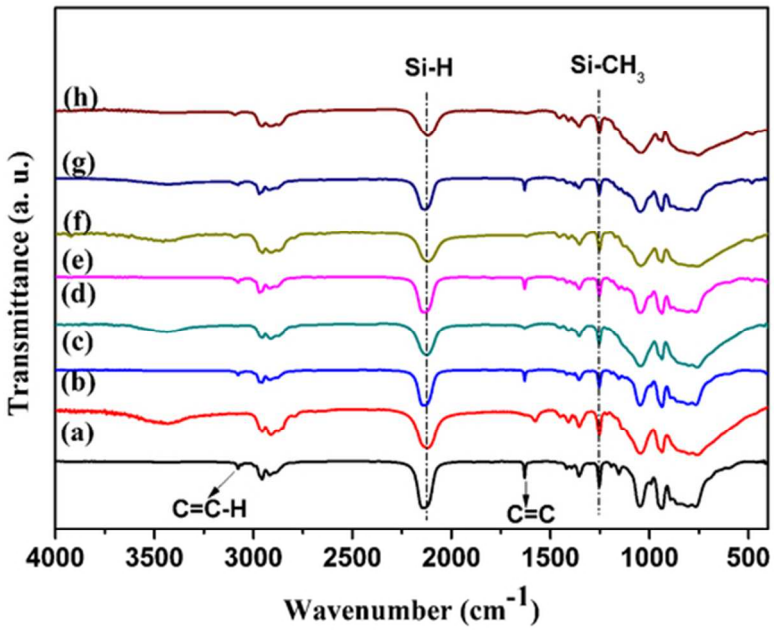

Fig.6. FT-IR spectra of (a) control AHPCS, (b) cured control AHPCS, (c) HBPFCS-1, (d) cured HBPFCS-1, (e) HBPFCS-3, (f) cured HBPFCS-3, (g) HBPFCS-5, and (h) cured HBPFCS-5 at 170 °C in Ar.
55x39mm (300 x 300 DPI)

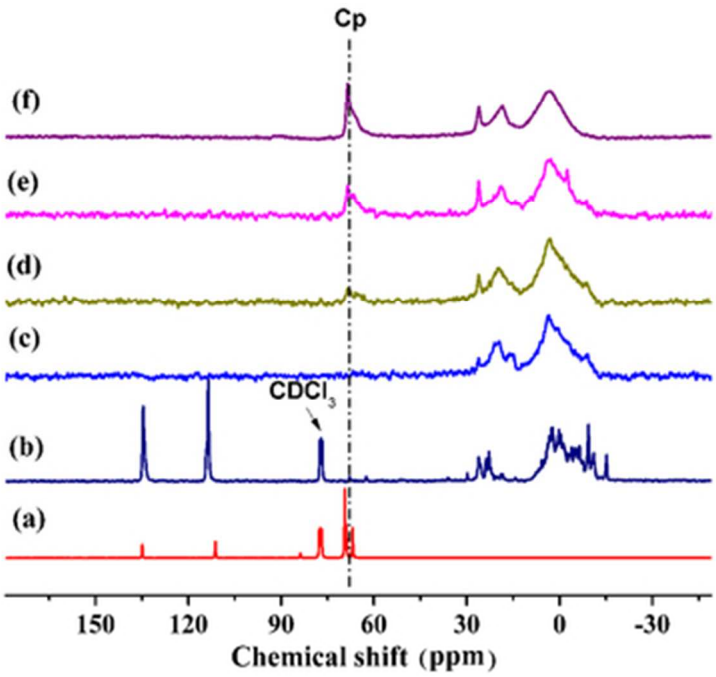

Fig.7. 13C NMR spectra of (a) VF, (b) parent AHPCS, and solid-state 13C MAS NMR spectra of cured (c) control AHPCS, (d) HBPFCS-1, (e) HBPFCS-3, (f) HBPFCS-5 at 170 °C in Ar.
41x29mm (300 x 300 DPI)

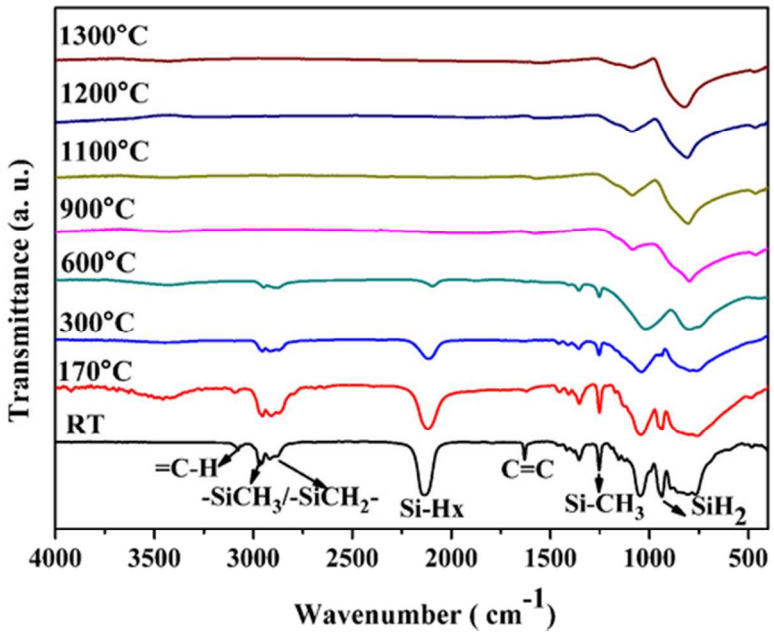

Fig.8. FT-IR spectra of HBPFCS-3 heat treated at different temperatures in Ar.
55x39mm (300 x 300 DPI)

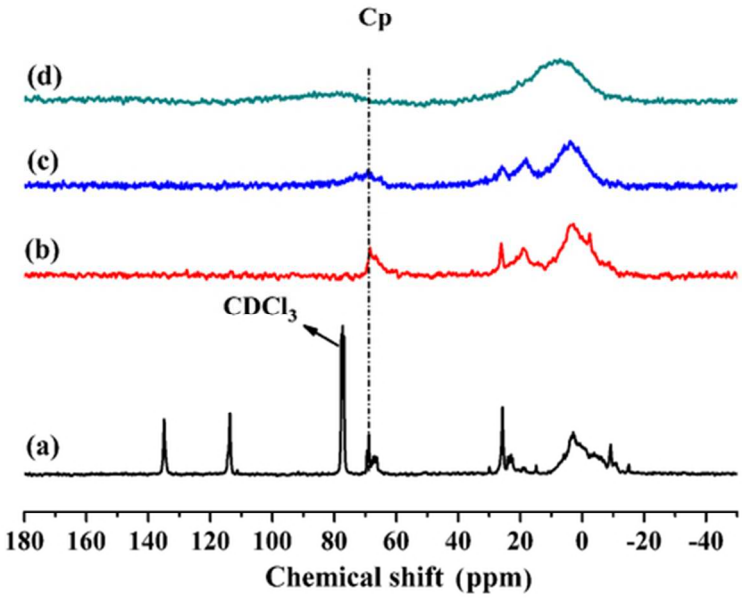

Fig.9. 13C NMR spectrum of (a) HBPFCS-3 and solid-state 13C MAS NMR spectra of samples pyrolyzed at various temperatures in Ar: (b) 170 °C, (c) 300 °C, and (d) 600 °C.

55x39mm (300 x 300 DPI)

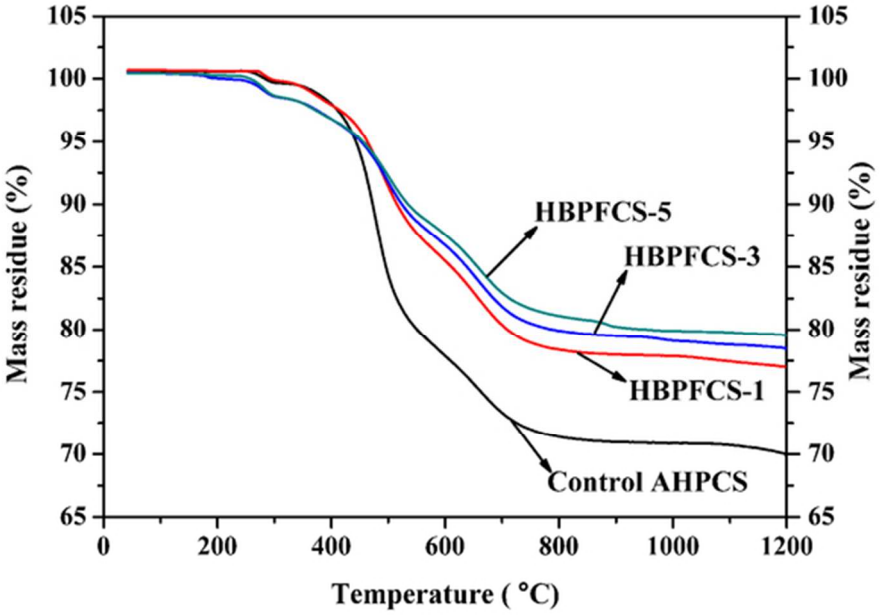

Fig.10. TGA curves of cured (a) control AHPCS, (b) HBPFCS-1, (c) HBPFCS-3, and (d) HBPFCS-5.
55x39mm (300 x 300 DPI)

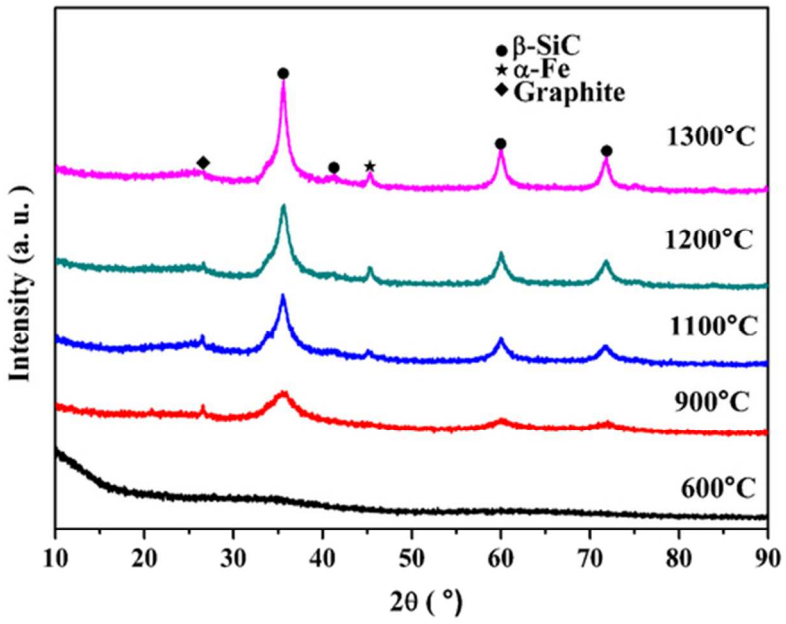

Fig.11. XRD patterns of HBPFCS-3-derived samples pyrolyzed at different temperatures.
55x39mm (300 x 300 DPI)

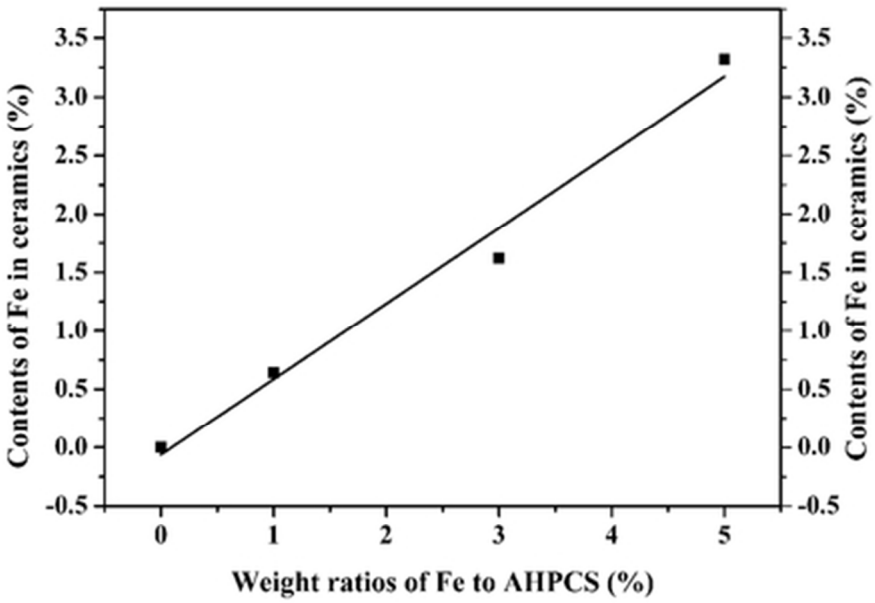

Fig.12. Dependence of the Fe content in the ceramics synthesized at 1300 °C on the iron content in feed.
41x29mm (300 x 300 DPI)

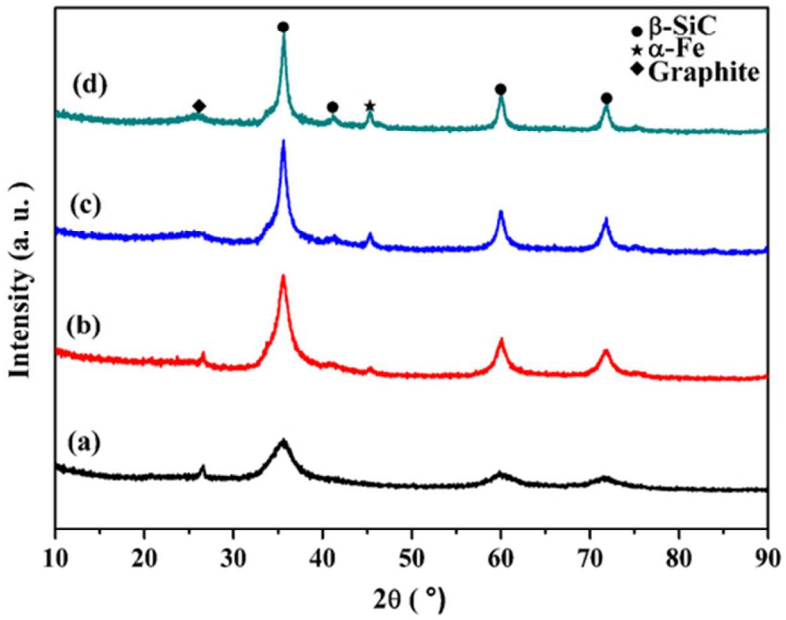

Fig.13. XRD patterns of 1300 °C ceramics derived from (a) control AHPCS, (b) HBPFCS-1, (c) HBPFCS-3, and (d) HBPFCS-5.
55x39mm (300 x 300 DPI)

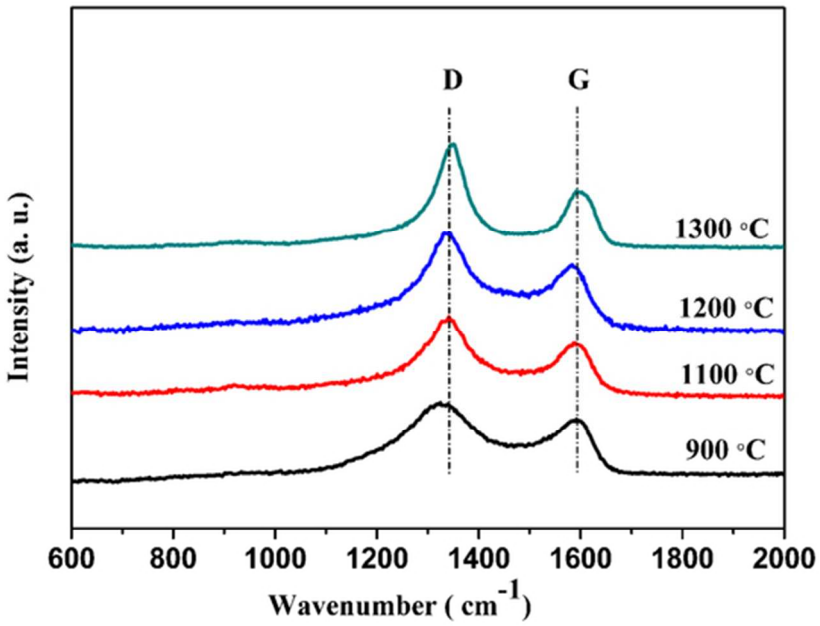

Fig. 14. Raman spectra of HBPFCS-3-derived ceramics at different temperatures.
55x39mm (300 x 300 DPI)

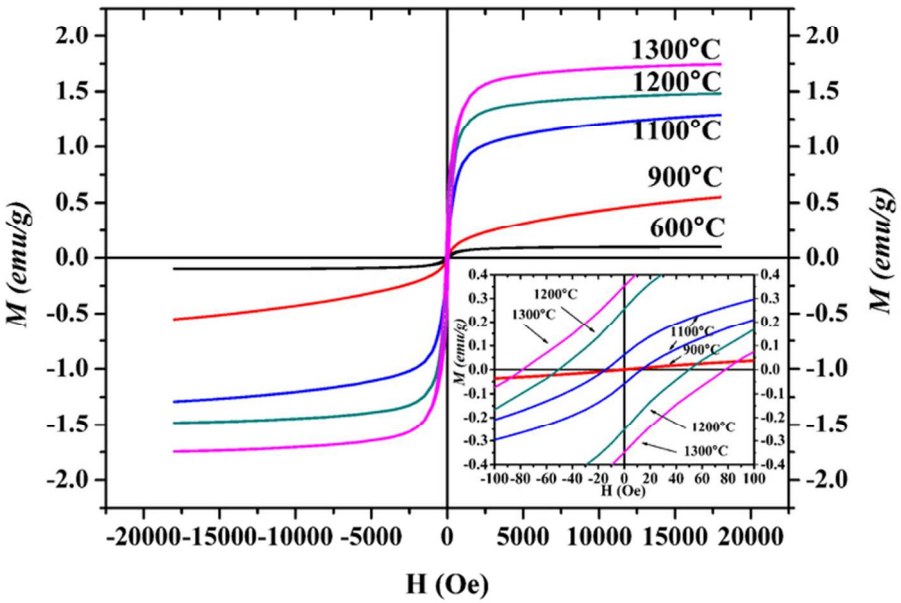

Fig.16. Magnetization versus applied magnetic field for HBPFCS-3-derived ceramics at different temperatures (inset: enlarged portion of the plots at low H).
69x48mm (300 x 300 DPI)

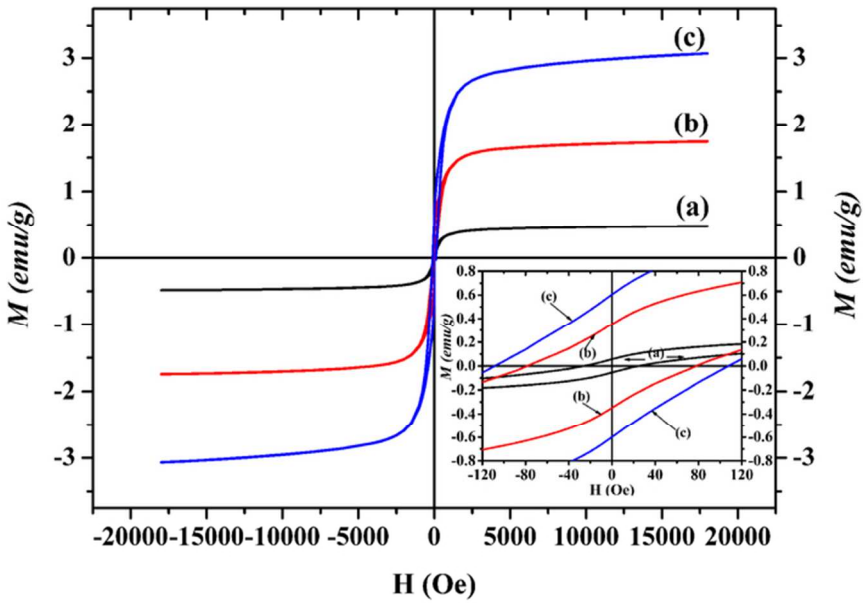

Fig.17. Magnetization versus applied magnetic field for 1300 °C ceramics derived from (a) HBPFCS-1, (b) HBPFCS-3, and (c) HBPFCS-5. (inset: enlarged portion of the plots at low H)
69x48mm (300 x 300 DPI)

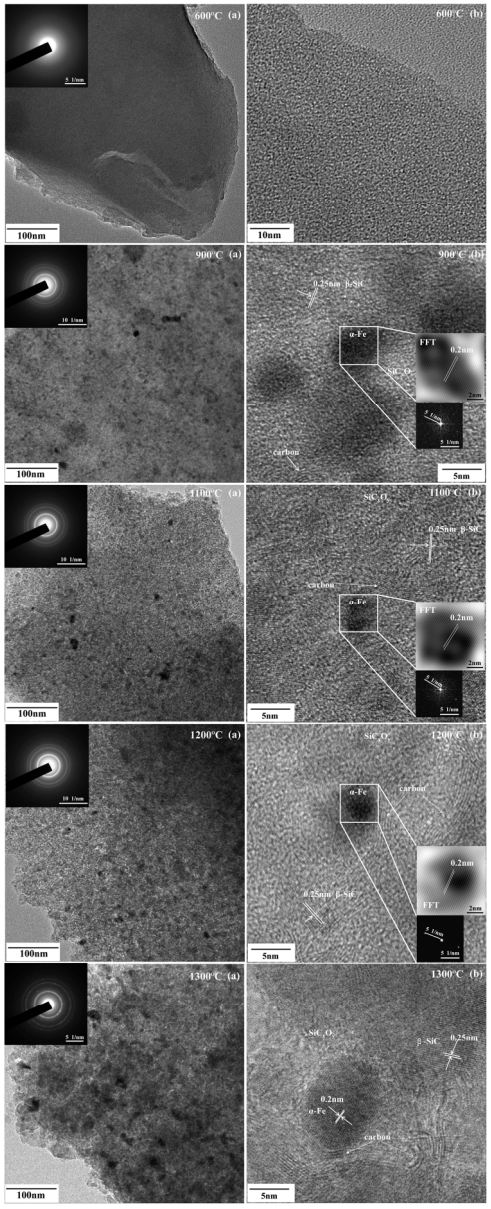

123x304mm (300 x 300 DPI)